CMS Physics Analysis Summary

Contact: cms-pag-conveners-higgs@cern.ch 2013/05/14

Search for the standard model Higgs boson produced in association with W or Z bosons, and decaying to bottom quarks (LHCP 2013)

The CMS Collaboration

Abstract

A search for the standard model Higgs boson (H) decaying to $b\bar{b}$, when produced in association with a weak vector boson (V), is reported for the following modes: W($\mu\nu$)H, W($e\nu$)H, W($\tau\nu$)H, Z($\mu\mu$)H, Z(ee)H and Z($\nu\nu$)H. The search is performed in data samples corresponding to integrated luminosities of 5.0 fb^{-1} at $\sqrt{s}$ =7 TeV and up to 19.0 fb^{-1} at $\sqrt{s}$ =8 TeV, recorded by the CMS experiment at the LHC. Upper limits, at the 95% confidence level, on the VH production cross section times the $H \to b\bar{b}$ branching ratio, with respect to the expectations for a standard model Higgs boson, are derived for a Higgs boson in the mass range 110-135 GeV. In this range, the observed upper limits vary from 1.1 to 3.1 times the standard model prediction; the corresponding expected limits vary from 0.7 to 1.5. At a Higgs boson mass of 125 GeV the observed limit is 1.89 and the expected limit is 0.95. An excess of events is observed above the expected background with a local significance of 2.1 standard deviations, consistent with the expectation from the production of the standard model Higgs boson. The signal strength corresponding to this excess, relative to that of the standard model Higgs boson, is $1.0^{+0.5}_{-0.5}$.

1 Introduction

The CMS and ATLAS collaborations have reported the discovery of a new boson [1, 2], with a mass, m_{H}, near 125 GeV and with properties compatible with those of the standard model Higgs boson [3–8]. To date, significant signals have been observed in channels where the boson decays into $\gamma\gamma$, ZZ and WW pairs. The interaction of this boson with the massive W and Z vector bosons indicates that it plays a role in electroweak symmetry breaking. The interaction with the fermions and whether the Higgs field serves as the source of mass generation in the fermion sector through a Yukawa interaction between the Higgs field and each fermion has not been firmly established.

At a mass of 125 GeV the standard model Higgs boson decays predominantly into a bottom-antibottom quark pair ($\mathrm{b\bar{b}}$). The observation and study of the $\mathrm{H} \to \mathrm{b\bar{b}}$ decay is therefore essential in determining the nature of the newly discovered boson. The measurement of $\mathrm{H} \to \mathrm{b\bar{b}}$ will be the first direct test of whether the observed boson interacts as expected with the quark sector, as the coupling to the top quark has, so far, only been tested through loop-level interactions. Recently, in a search for the standard model Higgs boson where the sensitivity below a mass of 130 GeV is dominated by the channels in which the Higgs boson is produced in association with a weak vector boson and decaying to $\mathrm{b\bar{b}}$, the CDF and D0 collaborations have reported evidence for an excess of events at a local significance of 3.1 standard deviations for a mass of 125 GeV [9].

In this note a search for the standard model Higgs boson in the $\mathrm{pp} \to \mathrm{VH}$ production mode is presented, where V is either a W or a Z boson and $\mathrm{H} \to \mathrm{b\bar{b}}$. The search is performed in data samples corresponding to integrated luminosities of 5.0 fb^{-1} at $\sqrt{s} = 7\,\mathrm{TeV}$ and up to 19.0 fb^{-1} at $\sqrt{s} = 8\,\mathrm{TeV}$, recorded by the CMS experiment at the LHC. The following six channels are included in the search: $\mathrm{W}(\mu\nu)\mathrm{H}$, $\mathrm{W}(e\nu)\mathrm{H}$, $\mathrm{W}(\tau\nu)\mathrm{H}$, $\mathrm{Z}(\mu\mu)\mathrm{H}$, $\mathrm{Z}(ee)\mathrm{H}$ and $\mathrm{Z}(\nu\nu)\mathrm{H}$, all with the Higgs boson decaying to $\mathrm{b\bar{b}}$. For the $\mathrm{W}(\tau\nu)\mathrm{H}$ final state, only the 8 TeV data is included and only those taus with 1-prong hadronic decays are explicitly considered; the τ notation throughout this note refers exclusively to such decays. The leptonic tau decays from taus in WH prcesses are implicitly included in the $\mathrm{W}(\mu\nu)\mathrm{H}$ and $\mathrm{W}(e\nu)\mathrm{H}$ channels. Backgrounds arise from production of W and Z bosons in association with jets (from all quark flavors), singly and pair-produced top quarks ($\mathrm{t\bar{t}}$), dibosons and QCD multijet processes.

Simulated samples of signal and backgrounds are used to provide guidance in the optimization of the analysis. Control regions in data are selected to adjust the event yields from simulation for the main background processes and to estimate their contribution in the signal region. Upper limits at the 95% confidence level (CL) on the $\mathrm{pp} \to \mathrm{VH}$ production cross section times the $\mathrm{H} \to \mathrm{b\bar{b}}$ branching ratio are obtained for Higgs boson masses in the 110–135 GeV range. These limits are extracted by fitting the shape of the distribution of the output discriminant of a boosted-decision-tree (BDT) discriminant [10] for the presence of a Higgs boson signal over what is expected from all background components. The significance of any excess of events over the prediction for the background is evaluated, and the corresponding event yield is compared with the expectaction from a standard model Higgs boson signal.

The analysis presented here contains approximately 7 fb^{-1} more 8 TeV data and includes some modifications with respect to the previous CMS Higgs boson search in these final states [11].

2 Detector and Simulations

A detailed description of the CMS detector can be found elsewhere [12]. The momenta of charged particles are measured using a silicon pixel and strip tracker that covers the pseudorapidity range $|\eta| < 2.5$ and is immersed in a 3.8 T solenoidal magnetic field. The pseudorapidity is defined as $\eta = -\ln(\tan(\theta/2))$, where θ is the polar angle of the trajectory of a particle with respect to the direction of the counterclockwise proton beam. Surrounding the tracker are a crystal electromagnetic calorimeter (ECAL) and a brass/scintillator hadron calorimeter (HCAL), both used to measure particle energy depositions and consisting of a barrel assembly and two endcaps. The ECAL and HCAL extend to a pseudorapidity range of $|\eta| < 3.0$. A steel/quartz-fiber Cherenkov forward detector (HF) extends the calorimetric coverage to $|\eta| < 5.0$. The outermost component of the CMS detector is the muon system consisting of gas detectors placed in the steel return yoke to measure the momentum of muons traversing through the detector.

Simulated samples of signal and backgrounds are produced using various event generators, with the CMS detector response modeled with GEANT4 [13]. The Higgs boson signal samples are produced using the POWHEG [14] event generator interfaced with HERWIG++ [15] for parton showering and hadronization. The MADGRAPH 5.1 [16] generator is used for the diboson, W+jets, Z+jets, and $t\bar{t}$ samples. The single-top samples are produced with POWHEG and the QCD multijet samples with PYTHIA. The default set of parton distribution functions (PDF) used to produce the Next-to-Leading-Order (NLO) POWHEG samples is the NLO MSTW2008 [17] while the Leading-Order (LO) CTEQ6L1 [18] is used for the rest of the samples, which come from LO calculations. The PYTHIA parameters for the underlying event are set to the Z2 tune for the 7 TeV samples and to Z2Star for the 8 TeV samples [19].

During the 2011 data taking period the LHC instantaneous luminosity reached up to $3.5 \times 10^{33}\text{cm}^{-2}\text{s}^{-1}$ and the average number of pp interactions per bunch crossing was approximately ten. During the 2012 period the LHC instantaneous luminosity reached $7.7 \times 10^{33}\text{cm}^{-2}\text{s}^{-1}$ and the average number of pp interactions per bunch crossing was approximately 21. Additional pp interactions overlapping with the event of interest in the same bunch crossing, denoted as pile-up events (PU), are therefore added in the simulated samples to represent the PU distribution measured in data.

3 Triggers

Several triggers are used to collect events consistent with the signal hypothesis in the six channels under consideration. For the W($\mu\nu$)H and W(eν)H channels the trigger paths consist of several single-lepton triggers with tight lepton identification. Leptons are also required to be isolated from other tracks and calorimeter energy depositions to maintain an acceptable trigger rate. For the W($\mu\nu$)H channel, for the 2011 data, the trigger thresholds for the muon transverse momentum, p_{T}, are in the range of 17 to 40 GeV. The higher thresholds are used for the periods of higher instantaneous luminosity. For the 2012 data the muon p_{T} trigger thresholds were set at 24 GeV for the single isolated-muon trigger. A single-muon trigger with a 40 GeV p_{T} threshold was also used, without any isolation requirements. The combined single-muon trigger efficiency is $\approx 90\%$ for signal events that pass all offline requirements that are described in section 5. For the W(eν)H channel, for the 2011 data, the electron p_{T} threshold ranges from 17 to 30 GeV. To maintain acceptable trigger rates during the periods of high instantaneous luminosity, the lower-threshold paths require two jets and a minimum requirement, in the 15–25 GeV range, on the magnitude of an online estimate the missing transverse energy vector,

$E_{\mathrm{T}}^{\mathrm{miss}}$. This variable is defined as the negative vector sum of the transverse momenta of all reconstructed jets identified by a particle-flow algorithm [20, 21]. The particle-flow algorithm combines the information from all CMS subdetectors to identify and reconstruct the individual particles emerging from any interaction vertex vertices: charged hadrons, neutral hadrons, photons, muons, and electrons. These particles are then used to reconstruct the missing transverse energy, jets, and hadronic τ-lepton decays, and to quantify the isolation of leptons and photons. For the 2012 data, the single isolated-electron trigger uses a 27 GeV threshold. The combined efficiency for these triggers for signal events that pass the final offline selection criteria is >95%.

For the W($\tau\nu$)H channel trigger, a 1-prong hadronically-decaying tau is required. The track p_{T} of the charged candidate coming from the tau decay is required to be above 20 GeV and the p_{T} threshold of the tau above 35 GeV. Additionally, the tau is required to be isolated inside a cone of 0.3, centered around the leading charged track, where there are no reconstructed particle-flow charged candidates with $p_{\mathrm{T}} > 1.5$ GeV and no particle-flow photon candidates with $E_{\mathrm{T}} > 2.0$ GeV. A further requirement of a minimum of 70 GeV is placed on the $E_{\mathrm{T}}^{\mathrm{miss}}$. The efficiency for this trigger for signal events that pass the final offline selection criteria is >90%.

The Z($\mu\mu$)H channel uses the same single-muon triggers as the W($\mu\nu$)H channel. For the Z(ee)H channel, dielectron triggers with lower p_{T} thresholds, of 17 and 8 GeV, and tight isolation requirements are used. These triggers are $\approx$ 99% efficient for all ZH signal events that pass the final offline selection criteria.

For the Z($\nu\nu$)H channel, combinations of several triggers are used, all with the requirement that the $E_{\mathrm{T}}^{\mathrm{miss}}$ be above a given threshold. Extra requirements are added to keep the trigger rates low as the luminosity increases and to reduce the $E_{\mathrm{T}}^{\mathrm{miss}}$ thresholds in order to increase signal acceptance. A trigger with $E_{\mathrm{T}}^{\mathrm{miss}} > 150$ GeV is used for the complete data set in both 2011 and 2012. During 2011 this trigger was used in conjunction with triggers that require the presence of two central jets ($|\eta| < 2.6$) with $p_{\mathrm{T}} > 20$ GeV and $E_{\mathrm{T}}^{\mathrm{miss}}$ thresholds of 80 or 100 GeV, depending on the luminosity. During 2012 this trigger was used in conjunction with a trigger that required two central jets with $p_{\mathrm{T}} > 30$ GeV and of $E_{\mathrm{T}}^{\mathrm{miss}} > 80$ GeV. This last trigger was discontinued when the instantaneous luminosity exceeded $3 \times 10^{33}\mathrm{cm}^{-2}\mathrm{s}^{-1}$ and was replaced by a trigger that requires missing transverse energy > 100 GeV, at least one pair of central jets with vectorial sum $p_{\mathrm{T}} > 100$ GeV and individual p_{T} above 60 and 25 GeV respectively, and no jet with $p_{\mathrm{T}} > 40$ GeV closer than 0.5 in azimuthal angle to the missing transverse energy direction. In order to increase signal acceptance at lower values of $E_{\mathrm{T}}^{\mathrm{miss}}$, triggers that require jets to be identified as coming from b quarks are used. For these triggers, two central jets with p_{T} above 20 or 30 GeV, depending on the luminosity conditions, are required. It is also required that at least one central jet with p_{T} above 20 GeV be tagged by the online Combined Secondary Vertex (CSV) b-tagging algorithm described in section 4. The $E_{\mathrm{T}}^{\mathrm{miss}}$ is required to be greater than 80 GeV for these triggers.

For Z($\nu\nu$)H events with $E_{\mathrm{T}}^{\mathrm{miss}} > 170$ GeV, the combined trigger efficiency for Z($\nu\nu$)H signal events is near 100% with respect to the offline event reconstruction and selection, described in the next section. For Z($\nu\nu$)H events with $E_{\mathrm{T}}^{\mathrm{miss}}$ between 130 and 170 GeV the corresponding efficiency is about 99%, and for events with $E_{\mathrm{T}}^{\mathrm{miss}}$ between 100 and 130 GeV the efficiency is 88%.

4 Event Reconstruction

The characterization of VH events, in the final states studied here, requires the reconstruction of the following objects, all originating from a common interaction vertex: Electrons, muons, taus and neutrinos (reconstructed as $E_{\mathrm{T}}^{\mathrm{miss}}$) –coming from the vector boson decays, and jets from b quarks –from the Higgs boson decays.

The reconstructed interaction vertex with the largest value of $\sum_i p_{\mathrm{T}i}^2$, where $p_{\mathrm{T}i}$ is the transverse momentum of the i-th track associated with the vertex, is selected as the primary event vertex. This vertex is used as the reference vertex for all relevant objects in the event, which are reconstructed with the particle-flow algorithm. The pile-up interactions affect jet momentum reconstruction, missing transverse energy reconstruction, lepton isolation and b-tagging efficiency. To mitigate these effects, a track-based algorithm that filters all charged hadrons that do not originate from the primary interaction is used. In addition, a calorimeter-based algorithm evaluates the energy density in the calorimeter from interactions not related to the primary vertex and subtracts it from reconstructed jets in the event [22].

Jets are reconstructed from particle-flow objects using the anti-k_T clustering algorithm [23], as implemented in the FASTJET package [24, 25], with a distance parameter of 0.5. Each jet is required to lie within $|\eta| < 2.5$, to have at least two tracks associated to it, and to have electromagnetic and hadronic energy fractions of at least 1% of the total jet energy. Jet energy corrections, as a function of pseudorapidity and transverse momentum of the jet, are applied [26]. The missing transverse energy vector is calculated offline as the negative of the vectorial sum of transverse momenta of all particle-flow objects identified in the event, and the magnitude of this vector is referred to as $E_{\mathrm{T}}^{\mathrm{miss}}$ in the rest of this note.

Electron reconstruction requires the matching of an energy cluster in the ECAL with a track in the silicon tracker [27]. Identification criteria based on the ECAL shower shape, track-ECAL cluster matching, and consistency with the primary vertex are imposed. Electron identification relies on a multivariate technique that combines observables sensitive to the amount of bremsstrahlung along the electron trajectory, the geometrical and momentum matching between the electron trajectory and associated clusters, as well as shower-shape observables. Additional requirements are imposed to remove electrons produced by photon conversions. In this analysis, electrons are considered in the pseudorapidity range $|\eta| < 2.5$, excluding the $1.44 < |\eta| < 1.57$ transition region between the ECAL barrel and endcap.

Muons are reconstructed using two algorithms [28]: one in which tracks in the silicon tracker are matched to signals in the muon chambers, and another in which a global track fit is performed seeded by signals in the muon system. The muon candidates used in the analysis are required to be reconstructed successfully by both algorithms. Further identification criteria are imposed on the muon candidates to reduce the fraction of tracks misidentified as muons. These include the number of measurements in the tracker and the muon system, the fit quality of the global muon track, and its consistency with the primary vertex. Muon candidates are considered in the $|\eta| < 2.4$ range.

Taus are reconstructed using the Hadron Plus Strips (HPS) algorithm [29] which uses charged hadrons and neutral electromagnetic objects ("photons") to reconstruct tau decays. In the first step of reconstruction, charged hadrons are reconstructed using the particle-flow algorithm. Next, since neutral pions are often produced in hadronic tau decays, the HPS algorithm is optimized to reconstruct π^0's in the ECAL as objects called strips. The strip reconstruction starts by centering one strip on the most energetic electromagnetic particle and then looking for other particles in a window of 0.05 in η and 0.20 in ϕ. Strips satisfying a minimum transverse mo-

mentum of $p_T^{strip} > 1$ GeV are combined with the charged hadrons to reconstruct the hadronic tau lepton. In the final step of reconstruction, all the charged hadrons and strips are required to be contained within a narrow cone size of $\Delta R = 2.8/p_T^{\tau}$, where p_T^{τ} is measured from the reconstruced charged hadron plus strips. Further identification criteria is imposed on the tau candidate to reduce the fraction of electron and muons faking taus. These include the tau candidate passing the anti-electron discriminator and an anti-muon discriminator. Additionally, the tau is required to be in the range $|\eta| < 2.1$. The tau reconstruction efficiency is approximately 50% while the misidentification rate from jets is about 1%.

Charged leptons from W and Z boson decays are expected to be isolated from other activity in the event. For each lepton candidate, a cone is constructed around the track direction at the event vertex. The scalar sum of the transverse momentum of each reconstructed particle compatible with the primary vertex and contained within the cone is calculated excluding the contribution from the lepton candidate itself. If this sum exceeds approximately 10% of the candidate p_{T}, the lepton is rejected; the exact requirement depends on the lepton η, p_{T} and its flavor. Including the isolation requirement, the total efficiency to reconstruct muons is in the 87–91% range, depending on p_{T} and η. The corresponding efficiencies for electrons are in the 81–98% range,

The CSV b-tagging algorithm [30] is used to identify jets that are likely to originate from the hadronization of b quarks. This algorithm combines in an efficient way the information about track impact parameters and secondary vertices within jets in a likelihood discriminant to provide separation of b jets from jets originating from light quarks, gluons and charm quarks. The efficiency to tag b jets and the rate of misidentification of non-b jets depend on the operating point chosen, and are typically parametrized as a function of the transverse momentum and pseudorapidity of the jets. These performance measurements are obtained directly from data in samples that can be enriched in b jets, such as $\mathrm{t\bar{t}}$ and multi-jet events (where, for example, requiring the presence of a muon in the jets enhances its heavy-flavor content). Several working points for the CSV output discriminant (which can have values between zero and one) are used in the analysis. For a CSV > 0.90 requirement the efficiencies to tag b quarks, c quarks, and light quarks or gluons are approximately 50%, 6%, and 0.15%, respectively [30]. The corresponding efficiencies for CSV > 0.50 are approximately 72%, 23%, and 3%.

All events from data and from the simulated samples are required to pass the same triggers and event reconstruction algorithms. Scale factors that account for the differences in the performance of these algorithms between data and simulations are computed and used in the analysis.

5 Event Selection

The background processes to VH production are vector-boson+jets (V+jets), $\mathrm{t\bar{t}}$, single-top, dibosons (VV) and QCD multijet production. Except for dibosons, these processes have production cross sections that are several orders of magnitude larger than Higgs boson production. The diboson production cross section is only a few times larger than the production cross section for VH and, given the nearly identical final state for VZ with $\mathrm{Z} \to \mathrm{b\bar{b}}$, this process provides a benchmark against which the Higgs boson search strategy can be tested.

The event selection is based on the kinematic reconstruction of the vector bosons in their leptonic decay modes and of the Higgs boson decay into two b-tagged jets. Backgrounds are substantially reduced by requiring a significant boost of the p_{T} of the vector boson, $p_{\mathrm{T}}(\mathrm{V})$, or the Higgs boson [31]. In that case the two particles recoil away from each other with a

large azimuthal opening angle, $\Delta\phi(\mathrm{V,H})$, between them. For each channel, different regions of $p_{\mathrm{T}}(\mathrm{V})$ boost are considered. Due to different signal and background composition, each boost region has different sensitivity and the analysis is performed separately in each region. The results from all regions are then combined for each channel. The "low", "intermediate", and "high" boost regions for the $\mathrm{W}(\mu\nu)\mathrm{H}$ and $\mathrm{W}(\mathrm{e}\nu)\mathrm{H}$ channels are $100 < p_{\mathrm{T}}(\mathrm{V}) < 130$ GeV, $130 < p_{\mathrm{T}}(\mathrm{V}) < 180$ GeV, and $p_{\mathrm{T}}(\mathrm{V}) > 180$ GeV. For the $\mathrm{W}(\tau\nu)\mathrm{H}$ a single $p_{\mathrm{T}}(\mathrm{V}) > 120$ GeV region is considered. For the $\mathrm{Z}(\nu\nu)\mathrm{H}$ channel the "low", "intermediate", and "high" boost regions are $100 < p_{\mathrm{T}}(\mathrm{V}) < 130$ GeV, $130 < p_{\mathrm{T}}(\mathrm{V}) < 170$ GeV and $p_{\mathrm{T}}(\mathrm{V}) > 170$ GeV, and for the $\mathrm{Z}(\ell\ell)\mathrm{H}$ channels, the "low" and "high" regions are $50 < p_{\mathrm{T}}(\mathrm{V}) < 100$ GeV and $p_{\mathrm{T}}(\mathrm{V}) > 100$ GeV.

Candidate $\mathrm{W} \to \ell\nu$ decays are identified by requiring the presence of a single isolated lepton and additional missing transverse energy. Muons are required to have a p_{T} above 20 GeV; the corresponding thresholds for electrons and taus are 30 GeV and 40 GeV, respectively. For the $\mathrm{W}(\ell\nu)\mathrm{H}$ and $\mathrm{W}(\tau\nu)\mathrm{H}$ channels, $E_{\mathrm{T}}^{\mathrm{miss}}$ is required to be greater than 45 GeV and 80 GeV, respectively, to reduce contamination from QCD multijet processes. To further reduce this contamination, it is also required for the $\mathrm{W}(\ell\nu)\mathrm{H}$ channels that the azimuthal angle between the $E_{\mathrm{T}}^{\mathrm{miss}}$ and the lepton be smaller than $\pi/2$, and that the lepton isolation for the low $p_{\mathrm{T}}(\mathrm{V})$ bin be tighter.

Candidate $\mathrm{Z} \to \ell\ell$ decays are reconstructed by combining isolated, oppositely charged pairs of electrons or muons and requiring the dilepton invariant mass to satisfy $75 < m_{\ell\ell} < 105$ GeV. For Z candidates the lepton p_{T} is required to be greater than 20 GeV. The identification of $\mathrm{Z} \to \nu\bar{\nu}$ decays requires the $E_{\mathrm{T}}^{\mathrm{miss}}$ in the event to be within the $p_{\mathrm{T}}(\mathrm{V})$ regions described above. The QCD multijet background is reduced to negligible levels in this channel when requiring that the $E_{\mathrm{T}}^{\mathrm{miss}}$ does not originate from mismeasured jets. To that end three event requirements are made. First, for the high $p_{\mathrm{T}}(\mathrm{V})$ boost region, a $\Delta\phi(\mathrm{E_T^{miss}}, \mathrm{jet}) > 0.5$ radians requirement is applied on the azimuthal angle between the $E_{\mathrm{T}}^{\mathrm{miss}}$ direction and the closest jet with $|\eta| < 2.5$ and $p_{\mathrm{T}} > 20$ GeV for the 7 TeV analysis or $p_{\mathrm{T}} > 25$ GeV for the 8 TeV analysis (where more pile-up is present). For the low and intermediate boost regions the requirement is increased to $\Delta\phi(\mathrm{E_T^{miss}}, \mathrm{jet}) > 0.7$ radians. The second requirement is that the azimuthal angle between the missing transverse energy as calculated from charged tracks only (with $p_{\mathrm{T}} > 0.5$ GeV and $|\eta| < 2.5$) and the $E_{\mathrm{T}}^{\mathrm{miss}}$, $\Delta\phi(\mathrm{E_T^{miss}}, \mathrm{E_T^{miss\,(trks)}})$, should be smaller than 0.5 radians. The third requirement is made for the low $p_{\mathrm{T}}(\mathrm{V})$ bin where the $E_{\mathrm{T}}^{\mathrm{miss}}$ significance (defined as the ratio between the $E_{\mathrm{T}}^{\mathrm{miss}}$ and the square root of the total transeverse energy in the calorimeter) should be larger than 3. Finally, to reduce backgrounds from $\mathrm{t\bar{t}}$ and WZ in the $\mathrm{W}(\ell\nu)\mathrm{H}$, $\mathrm{W}(\tau\nu)\mathrm{H}$, and $\mathrm{Z}(\nu\nu)\mathrm{H}$ channels, events with additional isolated leptons, N_{al}, with $p_{\mathrm{T}} > 20$ GeV are rejected.

The reconstruction of the $\mathrm{H} \to \mathrm{b\bar{b}}$ decay is made by requiring the presence of two central ($|\eta| < 2.5$) jets above a minimum p_{T} threshold, and tagged by the CSV algorithm, requiring that the value of the CSV discriminator be above a certain threshold. If more than two such jets are found in the event, the pair of jets with the highest vectorial sum of transverse momenta, $p_{\mathrm{T}}(\mathrm{jj})$, is selected. After the b-tagging requirements are applied, the fraction of $\mathrm{H} \to \mathrm{b\bar{b}}$ candidates in signal events that contain the two true b jets from the Higgs boson decay is near 100%. The background from V+jets and dibosons is reduced significantly through b tagging, and sub-processes where the two jets originate from genuine b quarks dominate the final selected data sample. After all event selection criteria described in this section are applied, the dijet invariant mass resolution of the two b jets from the Higgs decay is approximately 10%, with a few percent bias on the mass.

The Higgs boson mass resolution is improved by applying regression techniques similar to those used at the CDF experiment [32]. A further correction, beyond the standard CMS jet energy corrections, is computed for individual b jets in an attempt to recalibrate to the true parton energy. For this purpose, a specialized BDT discriminant is trained on simulated $H \to b\bar{b}$ signal events with inputs that include detailed information about the jet structure and that help differentiate jets from b quarks from light-flavor jets. These include variables containing information about several properties of a secondary vertex (when present), information about tracks, jet constituents, and other variables related to the energy reconstruction of the jet. In the cases where a soft lepton is found in or nearby the jet, the p_T of the lepton, the distance between the lepton and the jet and the momentum of the lepton transverse to the jet direction are also included in the BDT regression. For the $Z(\ell\ell)H$ channels the E_T^{miss} in the event and the azimuthal angle between the E_T^{miss} and each jet are also considered in the regression. The improvement on the mass resolution is approximately 15%, resulting in an increase in the analysis sensitivity of 10–20%, depending on the specific channel.

In the final stage of the analysis, to better separate signal from background under different Higgs boson mass hypotheses, another BDT discriminant is trained separately at each mass value using simulated samples for signal and all background processes that pass the event selection described above. The set of input variables used is chosen by iterative optimization from a larger number of potentially discriminating variables. Table 1 lists these variables. Jets are counted as additional jets if they satisfy the following: $p_T > 20$ GeV and $|\eta| < 4.5$ for $W(\ell\nu)H$, $p_T > 20$ GeV and $|\eta| < 2.5$ for $Z(\ell\ell)H$, and $p_T > 25$ GeV and $|\eta| < 4.5$ for $Z(\nu\nu)H$. The event selection requirements that are applied on all samples before training the BDT discriminant are listed in Table 2.

It has been been suggested that variables related to tecnhiques that study in more detail the substructure of jets could help improve the sensitivity of the $H \to b\bar{b}$ searches [31]. In this analysis, the addition of several combinations of such variables as inputs to the BDT discriminant did not result in any significant gains in sensitivity and are not included in the training used.

The shape of the output distribution of this BDT discriminant is the final discriminant on which a fit is performed to search for events resulting from Higgs boson production. Before testing all events through this final BDT discriminant, events are classified based on where they fall in the output distributions of several other BDT discriminants that are trained to discern signal from specific backgrounds. This technique, similar to the one used by the CDF collaboration in [33], divides the samples into four distinct subsets that are enriched in $t\bar{t}$, V+jets, dibosons, and VH. The increase in the analysis sensitivity from using this technique in the $Z(\nu\nu)H$ and $W(\ell\nu)H$ channels is 5–10%. For the $Z(\ell\ell)H$ channel the improvement is not significant and therefore the technique is not used for that case. The technique is also not used in the $W(\tau\nu)H$ channel due to the limited size of the Monte Carlo samples available for training several BDT discriminants. The first background-specific BDT discriminant is trained to separate $t\bar{t}$ from VH, the second one is trained to separate V+jets from VH, and the third one separates diboson background from VH. The output distributions of the background-specific BDTs are used to separate events in four categories: Those that fail a cut on the $t\bar{t}$ BDT are classified as $t\bar{t}$ -like events, those that pass the $t\bar{t}$ BDT cut but fail a cut on the V+jets BDT are classified as V+jets -like events, those that pass the V+jets BDT cut but fail the cut on the diboson BDT are classified as diboson-like events and, finally, those that pass all BDT cuts are VH-enriched events. The events in each category are then run through the final BDT discriminant and the resulting distribution, now composed of four distinct subsets of events, is used as input to the fitting program

Table 1: Variables used in the BDT training.

Variable
$p_T(j)$: transverse momentum of each Higgs daughter
$m(jj)$: dijet invariant mass
$p_T(jj)$: dijet transverse momentum
$p_T(V)$: vector boson transverse momentum (or E_T^{miss})
CSV_{max}: value of CSV for the Higgs daughter with largest CSV value
CSV_{min}: value of CSV for the Higgs daughter with second largest CSV value
$\Delta\phi(V,H)$: azimuthal angle between V (or E_T^{miss}) and dijet
$\lvert\Delta\eta(jj)\rvert$: difference in η between Higgs daughters
$\Delta R(jj)$: distance in η–ϕ between Higgs daughters
N_{aj}: number of additional jets
$\Delta\theta_{pull}$: color pull angle [34]
$\Delta\phi(E_T^{miss}, jet)$: azimuthal angle between E_T^{miss} and the closest jet (only for $Z(\nu\nu)H$)
$maxCSV_{aj}$: maximum CSV of the additional jets in an event (only for $Z(\nu\nu)H$ and $W(\ell\nu)H$)
$min\Delta R(H, aj)$: mimimum distance between an additional jet and the Higgs candidate (only for $Z(\nu\nu)H$ and $W(\ell\nu)H$)
Angular variables: HV system mass, Angle Z-Z*, Angle Z-l, Angle H-jet (only for $Z(\ell\ell)H$)

As a validation of the multi-variate approach to this analysis, these BDT discriminants are also trained to find diboson signals (ZZ and WZ, with $Z\rightarrow b\bar{b}$) rather than the VH production signal. The event selection used for this test is identical to that used for the VH search.

5.1 Dijet Mass Analysis

As a cross-check to the BDT-based analysis, a simpler analysis is done by performing a fit to the shape of the dijet invariant mass distribution, $m(jj)$, of the two jets associated to the reconstructed Higgs boson. The event selection for this analysis is more restrictive than the one used in the BDT analysis and is optimized for sensitivity in this single variable. Table 3 lists the event selection of the $m(jj)$analysis. Since the diboson background will also exhibit a peak in the $m(jj)$distribution, from Z bosons that decay into b quark pairs, the distribution is also used to measure the consistency of the diboson rate with that of the expectation from the standard model. This measurement validates the estimate of the backgrounds in the Higgs boson search.

6 Background Control Regions

Appropriate control regions are identified in data and used to correct the Monte Carlo yield estimates for several of the most important background processes: Production of W and Z bosons in association with jets (light- and heavy-flavor) and $t\bar{t}$ production. A set of simultaneous fits is then performed to several distributions of discriminating variables in the control regions, separately in each channel, to obtain consistent scale factors by which the Monte Carlo yields are adjusted. These scale factors account not only for cross section discrepancies, but also potential residual differences in physics object selection. Therefore, separate scale factors are used for each background process in the different channels. For the W and Z backgrounds the controls regions are defined such that they are enriched in either heavy-flavor (HF) or light-flavor (LF) jets. Furthermore, the scale factors for these processes are split according to how many of the two jets selected in the Higgs boson reconstruction originate from b quarks. The uncertainties in the scale factor determination include two components: The first is the statistical uncertainty coming from the fits (affected by the finite size of the samples), and the second is the systematic uncertainty obtained by refitting the distributions in the control regions after these are modified by the effect of various sources of systematic uncertainty such as b-tagging, jet energy

Table 2: Selection criteria for the samples used in the BDT training in each channel.Entries marked with "–" indicate that the variable is not used in the given channel. If different, the entries in parenthesis indicate the selection for the high-$p_{\mathrm{T}}(\mathrm{V})$ region for $\mathrm{Z}(\ell\ell)\mathrm{H}$ and the selection for the intermediate- and high-$p_{\mathrm{T}}(\mathrm{V})$ regions for $\mathrm{Z}(\nu\nu)\mathrm{H}$ and $\mathrm{W}(\ell\nu)\mathrm{H}$). The second and third rows refer to the p_{T} thresholds on the leading (j_1) and sub-leading (j_2) jets. $p_T(track)$ is transverse momentum of the leading tau track. The values listed for kinematical variables are in units of GeV.

Variable	$\mathrm{W}(\ell\nu)\mathrm{H}$	$\mathrm{W}(\tau\nu)\mathrm{H}$	$\mathrm{Z}(\ell\ell)\mathrm{H}$	$\mathrm{Z}(\nu\nu)\mathrm{H}$
$m_{\ell\ell}$	–	–	$[75-105]$	–
$p_{\mathrm{T}}(j_1)$	> 30	> 30	> 20	> 60
$p_{\mathrm{T}}(j_2)$	> 30	> 30	> 20	> 30
$p_{\mathrm{T}}(\mathrm{jj})$	> 100	> 120	–	> 100 (> 130,> 130)
$m(\mathrm{jj})$	< 250	< 250	$[40-250]$ (< 250)	< 250
$p_{\mathrm{T}}(\mathrm{V})$	$100-130$ ($130-180$,> 180)	> 120	$[50-100]$ (> 100)	–
$\mathrm{CSV}_{\mathrm{max}}$	> 0.40	> 0.40	> 0.50 (> 0.244)	> 0.679
$\mathrm{CSV}_{\mathrm{min}}$	> 0.40	> 0.40	> 0.244	> 0.244
N_{aj}	–	–	–	< 2 (–,–)
N_{al}	$= 0$	$= 0$	–	$= 0$
$E_{\mathrm{T}}^{\mathrm{miss}}$	> 45	> 80	–	$[100-130]$ ($[130-170]$,> 170)
$\Delta\phi(\mathrm{V},\mathrm{H})$	–	–	–	> 2.0
$\Delta\phi(\mathrm{E}_{\mathrm{T}}^{\mathrm{miss}},\mathrm{jet})$	–	–	–	> 0.7 (> 0.7, > 0.5)
$\Delta\phi(\mathrm{E}_{\mathrm{T}}^{\mathrm{miss}},\mathrm{E}_{\mathrm{T}}^{\mathrm{miss(trks)}})$	–	–	–	< 0.5
$E_{\mathrm{T}}^{\mathrm{miss}}$ significance	–	–	–	> 3 (–,–)
$\Delta\phi(\mathrm{E}_{\mathrm{T}}^{\mathrm{miss}},\ell)$	$< \pi/2$		–	–
$p_T(\tau)$	–	> 40	–	–
$p_T(track)$	–	> 20	–	–

Table 3: Selection criteria for the samples used in the $m(\mathrm{jj})$ analysis in each channel. Entries marked with "–" indicate that the variable is not used in the given channel. If different, the entries in parenthesis indicate the selection for the corresponding $p_{\mathrm{T}}(\mathrm{V})$ regions as defined in the $p_{\mathrm{T}}(\mathrm{V})$ row. The second and third rows refer to the p_{T} thresholds on the leading (j_1) and sub-leading (j_2) jets. $p_T(track)$ is transverse momentum of the leading tau track. The values listed for kinematical variables are in units of GeV.

Variable	$\mathrm{W}(\mu\nu)\mathrm{H}$	$\mathrm{W}(\mathrm{e}\nu)\mathrm{H}$	$\mathrm{W}(\tau\nu)\mathrm{H}$	$\mathrm{Z}(\ell\ell)\mathrm{H}$	$\mathrm{Z}(\nu\nu)\mathrm{H}$
$m_{\ell\ell}$	–	–	–	$75 < m_{\ell\ell} < 105$	–
$p_{\mathrm{T}}(j_1)$	> 30	> 30	> 30	> 20	> 60 (> 60, > 80)
$p_{\mathrm{T}}(j_2)$	> 30	> 30	> 30	> 20	> 30
$p_{\mathrm{T}}(\mathrm{jj})$	> 100	> 100	> 120	–	> 110 (> 140, > 190)
$p_{\mathrm{T}}(\mathrm{V})$	$100-130$ ($130-180$ > 180)	$[100-150]$(> 150)	< 250	$[50-100]$, ($[100-150]$, > 150)	–
$\mathrm{CSV}_{\mathrm{max}}$	0.898	0.898	0.898	0.679	0.898
$\mathrm{CSV}_{\mathrm{min}}$	> 0.5	> 0.5	> 0.4	> 0.5	> 0.5
$\Delta\phi(\mathrm{V},\mathrm{H})$	> 2.95	> 2.95	> 2.95	–	> 2.95
$\Delta R(\mathrm{jj})$	–	–	$= 0$	$-$, ($-$, < 1.6)	–
N_{aj}	$= 0$	$= 0$	$= 0$	–	$= 0$
N_{al}	$= 0$	$= 0$	> 80	–	$= 0$
$E_{\mathrm{T}}^{\mathrm{miss}}$	> 45	> 45	–	$< 60.$	$[100-130]$ ($[130-170]$, > 170)
$\Delta\phi(\mathrm{E}_{\mathrm{T}}^{\mathrm{miss}},\mathrm{jet})$	–	–	–	–	> 0.7 (> 0.7, > 0.5)
$\Delta\phi(\mathrm{E}_{\mathrm{T}}^{\mathrm{miss}},\mathrm{E}_{\mathrm{T}}^{\mathrm{miss(trks)}})$	–	–	–	–	< 0.5
$\Delta\phi(\mathrm{E}_{\mathrm{T}}^{\mathrm{miss}},\ell)$	$< \pi/2$	$< \pi/2$	–	–	–
$p_T(\tau)$	–	–	> 40	–	–
$p_T(track)$	–	–	> 20	–	–

Table 4: Definition of control regions for all the WH channels for the low and high $p_T(V)$ regions. The values in parenthesis are used for the intermediate and high $p_T(V)$ region. LF and HF refer to light- and heavy-flavor jets. N_{al} is the number of additional isolated leptons in the event. The values listed for kinematical variables are in units of GeV.

Variable	W+LF	$t\bar{t}$	W+HF
$p_T(j_1)$	> 30	> 30	> 30
$p_T(j_2)$	> 30	> 30	> 30
$p_T(jj)$	> 120	> 120	> 120
$p_T(V)$	$[100-130]$ ($[130,180] > 180$)	$[100-130]$ ($[130,180] > 180$)	$[100-130]$ ($[130,180] > 180$)
CSV_{max}	$[0.244-0.898]$	> 0.898	> 0.898
N_{aj}	< 2	> 1	$= 0$
N_{al}	$= 0$	$= 0$	$= 0$
E_T^{miss}	> 45	> 45	> 45
E_T^{miss} significance	$> 2.0(\mu)$ $> 3.0(e)$	–	–
$m(jj)$	< 250	< 250	veto $[90-150]$

Table 5: Definition of control regions for the $Z(\ell\ell)H$ channel. The same selection is used for both the low and high $p_T(V)$ regions. The values listed for kinematical variables are in units of GeV.

Variable	Z+jets	$t\bar{t}$
$m_{\ell\ell}$	$[75-105]$	veto $[75-105]$
$p_T(j_1)$	> 20	> 20
$p_T(j_2)$	> 20	> 20
$p_T(V)$	$[50-100]$	$[50-100]$
CSV_{max}	> 0.244	> 0.244
CSV_{min}	> 0.244	> 0.244
$m(jj)$	veto $[80-150]$, < 250	veto $[80-150]$, < 250

scale, and jet energy resolution.

Tables 4–6 list the selection criteria used for the control regions for the WH, $Z(\ell\ell)H$, and $Z(\nu\nu)H$ channels, respectively. Table 7 summarizes the fit results for all channels for 8 TeV data. The scale factors are found to be close to unity for all processes except for vector bosons with one b quark, for which the scale factor is of order two. In this sample most of the excess in the single b-tagged jet data occurs in the region where two displaced vertices are found relatively close to each other ($\Delta R < 0.5$). This discrepancy is interpreted as arising mainly from mismodeling of the generator parton shower in the gluon-splitting process to b-quark pairs. In this process the dominant contribution contains typically a soft b quark that can end up not being reconstructed as a jet above the p_T threshold used in the analysis, or that is merged with the jet from the more energetic b quark. These discrepancies are consistent with similar observations in other studies of vector boson with heavy-flavor by the CMS [35] and ATLAS [36] experiments.

7 Uncertainties

The results obtained in this analysis are: An upper limit on the production cross section of a standard model Higgs boson produced in association with a vector boson and decaying to a $b\bar{b}$ pair, the probability that any excess of events over background comes from background

Table 6: Definition of control regions for the $Z(\nu\nu)H$ channel for the low, intermediate and high $p_T(V)$ regions. The values in parenthesis are for the intermediate and high $p_T(V)$ regions. N_{al} is the number of additional isolated leptons in the event. The values listed for kinematical variables are in units of GeV.

Variable	Z+LF	Z+HF	$t\bar{t}$	W+LF	W+HF
$p_T(j_1)$	> 60	> 60	> 60	> 60	> 60
$p_T(j_2)$	> 30	> 30	> 30	> 30	> 30
$p_T(jj)$	> 100 (> 130,> 130)	> 100 (> 130,> 130)	> 100 (> 130,> 130)	> 100 (> 130,> 130)	> 100 (> 130,> 130)
$m(jj)$	< 250	< 250, veto $[100-140]$	250, veto $[100-140]$	< 250	< 250, veto $[100-140]$
$p_T(V)$	–	–	–	–	–
CSV_{max}	$[0.244-0.898]$	> 0.679	> 0.898	$[0.244-0.898]$	> 0.679
CSV_{min}	–	> 0.244	–	–	> 0.244
N_{aj}	< 2 (–,–)	< 2 (–,–)	≥ 1	$= 0$	$= 0$
N_{al}	$= 0$	$= 0$	$= 1$	$= 1$	$= 1$
E_T^{miss}	$[100-130]$ ($[130-170]$,> 170)	$[100-130]$ ($[130-170]$,> 170)	$[100-130]$ ($[130-170]$,> 170)	$[100-130]$ ($[130-170]$,> 170)	$[100-130]$ ($[130-170]$,> 170)
$\Delta\phi(V,H)$	–	> 2.0	–	–	> 2.0
$\Delta\phi(E_T^{miss}, jet)$	> 0.7 (> 0.7,> 0.5)	> 0.7 (> 0.7,> 0.5)	> 0.7 (> 0.7,> 0.5)	> 0.7 (> 0.7,> 0.5)	> 0.7 (> 0.7,> 0.5)
$\Delta\phi(E_T^{miss}, E_T^{miss(trks)})$	< 0.5	< 0.5	–	–	–
E_T^{miss} significance	> 3 (–,–)	> 3 (–,–)	> 3 (–,–)	> 3 (–,–)	> 3 (–,–)

Table 7: 8 TeV Data/MC scale factors for each control region in each decay mode. The errors include the statistical uncertainty from the fit, and a systematic uncertainty accounting for possible data/MC shape differences in the discriminating variables. Electron and muons samples in $Z(\ell\ell)H$ and $W(\ell\nu)H$ are fit simultaneously to determine average scale factors.

Process	$W(\ell\nu)H$	$Z(\ell\ell)H$	$Z(\nu\nu)H$
Low p_T			
W0b	$1.03 \pm 0.01 \pm 0.05$	–	$0.83 \pm 0.02 \pm 0.04$
W1b	$2.22 \pm 0.25 \pm 0.20$	–	$2.30 \pm 0.21 \pm 0.11$
W2b	$1.58 \pm 0.26 \pm 0.24$	–	$0.85 \pm 0.24 \pm 0.14$
Z0b	–	$1.11 \pm 0.04 \pm 0.06$	$1.24 \pm 0.03 \pm 0.09$
Z1b	–	$1.59 \pm 0.07 \pm 0.08$	$2.06 \pm 0.06 \pm 0.09$
Z2b	–	$0.98 \pm 0.10 \pm 0.08$	$1.25 \pm 0.05 \pm 0.11$
$t\bar{t}$	$1.03 \pm 0.01 \pm 0.04$	$1.10 \pm 0.05 \pm 0.06$	$1.01 \pm 0.02 \pm 0.04$
Intermediate p_T			
W0b	$1.02 \pm 0.01 \pm 0.07$	–	$0.93 \pm 0.02 \pm 0.04$
W1b	$2.90 \pm 0.26 \pm 0.20$	–	$2.08 \pm 0.20 \pm 0.12$
W2b	$1.30 \pm 0.23 \pm 0.14$	–	$0.75 \pm 0.26 \pm 0.11$
Z0b	–	–	$1.19 \pm 0.03 \pm 0.07$
Z1b	–	–	$2.30 \pm 0.07 \pm 0.08$
Z2b	–	–	$1.11 \pm 0.06 \pm 0.12$
$t\bar{t}$	$1.02 \pm 0.01 \pm 0.15$	–	$0.99 \pm 0.02 \pm 0.03$
High p_T			
W0b	$1.04 \pm 0.01 \pm 0.07$	–	$0.93 \pm 0.02 \pm 0.03$
W1b	$2.46 \pm 0.33 \pm 0.22$	–	$2.12 \pm 0.22 \pm 0.10$
W2b	$0.77 \pm 0.25 \pm 0.08$	–	$0.71 \pm 0.25 \pm 0.15$
Z0b	–	$1.11 \pm 0.04 \pm 0.06$	$1.17 \pm 0.02 \pm 0.08$
Z1b	–	$1.59 \pm 0.07 \pm 0.08$	$2.13 \pm 0.05 \pm 0.07$
Z2b	–	$0.98 \pm 0.10 \pm 0.08$	$1.12 \pm 0.04 \pm 0.10$
$t\bar{t}$	$1.00 \pm 0.01 \pm 0.11$	$1.10 \pm 0.05 \pm 0.06$	$0.99 \pm 0.02 \pm 0.03$

fluctuations alone (significance), and the most likely value of the production cross section for a 125 GeV Higgs boson, relative to the standard model cross section (signal strength). The systematic uncertainties that affect these results are listed in Table 8 and described in more detail in what follows.

The uncertainty in the CMS luminosity measurement is estimated to be 2.2% for the 2011 data [37] and 4.4% for the 2012 data [38]. Muon and electron trigger, reconstruction, and identification efficiencies are determined in data from samples of leptonic Z boson decays. The uncertainty on the yields due to the trigger efficiency is 2% per charged lepton and the uncertainty on the identification efficiency is also 2% per lepton. The parameters describing the $Z(\nu\nu)H$ trigger efficiency turn-on curve have been varied within their statistical uncertainties and for different assumptions on the methodology to derive the efficiency. A yield uncertainty of about 3% is estimated.

The jet energy scale is varied within one standard deviation as a function of jet p_T and η. The efficiency of the analysis selection is recomputed to assess the variation in yield. Depending on the process, a 2–3% yield variation is found. The effect of the uncertainty on the jet energy resolution is evaluated by smearing the jet energies according to the measured uncertainty. Depending on the process, a 3–6% variation in yields due to this effect is obtained. The uncertainties in the jet energy scale and resolution also have an effect on the shape of the BDT output distribution. The impact of the jet energy scale uncertainty is determined by recomputing the BDT distribution after shifting the energy scale up and down by its uncertainty. Similarly, the impact of the jet energy resolution is determined by recomputing the BDT distribution after increasing or decreasing the jet energy resolution. An uncertainty of 3% is assigned to the yields of all processes in the $W(\ell\nu)H$ and $Z(\nu\nu)H$ channels due to the uncertainty related to the missing transverse energy estimate.

Data-to-simulation b-tagging scale factors, measured in $t\bar{t}$ events, are applied consistently to jets in signal and background events. The measured uncertainties for the b-tagging scale factors are: 3% per b tag, 6% per charm tag, and 15% per mistagged jet (originating from gluons and light u, d, s quarks) [30]. These translate into yield uncertainties in the 3–15% range, depending on the channel and the specific process. The shape of the BDT output distribution is also affected by the shape of the CSV distribution and therefore recomputed according to an up and down range of variations of the CSV distributions.

The total VH signal cross section has been calculated to next-to-next-to-leading order (NNLO) accuracy, and the total theoretical uncertainty is 4% [39], including the effect of scale and PDF variations [17, 40–43]. This analysis is performed in the boosted regime, and thus, potential differences in the p_T spectrum of the V and H between data and Monte Carlo generators could introduce systematic effects in the signal acceptance and efficiency estimates. Two calculations are available that estimate the NLO electroweak [44–46] and NNLO QCD [47] corrections to VH production in the boosted regime. Both the EWK and NNLO QCD corrections are applied to the signal samples.The estimated uncertainties from the NNLO electroweak corrections are 2% for ZH and 2% for WH. For the NNLO QCD correction, an uncertainty of 5% for both ZH and WH is estimated.

The uncertainty in the background yields that results from the estimates from data is approximately 10%. For V+jets the difference in the shape of the BDT output distribution for events from the MADGRAPH and HERWIG++ Monte Carlo generators is considered as a shape uncertainty. For $t\bar{t}$ the BDT output shape difference between the nominal MADGRAPH and the POWHEG generators is considered as a shape systematic. Uncertainties of 15% are assigned to the yields obtained from simulation for single-top production in the t-channel and in the

Table 8: Information about each source of systematic uncertainty, including whether it affects the shape or normalization of the BDT output, the uncertainty on signal or background yields, and the relative contribution to the uncertainty on the signal strength. Due to correlations, the total systematic uncertainty is less than the sum in quadrature of the individual uncertainties. The last column shows the percentage decrease in the total signal strength uncertainty, including statistical, when removing that specific source of uncertainty. The ranges quoted are due to variations from 7 and 8 TeV data, different decay modes, specific background processes, and the different Higgs boson mass hypotheses.

Source	Type	Yield uncertainty (%) range	Contribution to uncertainty (%)	Removal effect on total uncertainty (%)
Luminosity	normalization	2.2-4.4	< 2	< 0.1
Lepton efficiency and trigger (per lepton)	normalization	3	< 2	< 0.1
$Z(\nu\nu)H$ triggers	shape	3	< 2	< 0.1
Jet energy scale	shape	2–3	5.0	0.5
Jet energy resolution	shape	3–6	5.9	0.7
Missing transverse energy	shape	3	3.2	0.2
b-tagging	shape	3–15	10.2	2.1
Signal cross section (scale and PDF)	normalization	4	3.9	0.3
Signal cross section (p_T boost, EWK/QCD)	normalization	2/5	3.9	0.3
Signal Monte Carlo statistics	shape	1–5	13.3	3.6
Backgrounds (data estimate)	normlization	10	15.9	5.2
Single-top (simulation estimate)	normalization	15	5.0	0.5
Dibosons (simulation estimate)	normalization	15	5.0	0.5
MC modeling (V+jets and $t\bar{t}$)	shape	10	7.4	1.1

tW-channel, respectively. For the diboson backgrounds, a 15% cross section uncertainty is assumed. These uncertainties are consistent with the CMS measurements of these processes in [48] and [49], respectively.

The combined effect of the systematic uncertainties results in an increase of about 15% on the expected upper limit on the Higgs boson production cross section and in a reduction of 15% on the expected significance of an observation when the Higgs boson is present in the data at the predicted standard model rate.

8 Results

Results are obtained from combined signal and background fits to the shape of the output distributions of the BDT discriminants trained separately for each channel and for each Higgs boson mass hypothesis in the 110–135 GeV range examined. In the fit the BDT shape and normalization, for signal and for each background component, are allowed to vary within the systematic and statistical uncertainties described in section 7. These uncertainties are treated as nuisance parameters in the fit, with appropriate correlations taken into account. All nuisance parameters, including the scale factors described in section 6 get adjusted by the fit.

Figure 1 shows an example of these BDT distributions, for the m_H= 125 GeV training, for the high $p_T(V)$ bin of the $Z(\nu\nu)H$ channel. The adjusted scale factors have been applied. The four partitions in the figure on the left correspond to the subsets enriched in $t\bar{t}$, vector-boson+jets, dibosons and finally, VH -as described in section 5. The figure on the right shows the last, VH-enriched, partition in more detail. For completeness, all the BDT distributions are shown in Figs. 6–10, in appendix 10. Fig. 2 combines all these discriminants into a single distribution where all events, for all channels, are sorted in bins of similar expected signal-to-background ratio, as given by the value of the output of their corresponding BDT discriminant (trained

with a Higgs boson mass of 125 GeV). The observed excess of events in the bins with the largest signal-to-background ratio is consistent with what is expected from the production of a standard model Higgs boson.

The results of all channels, for all $p_{\mathrm{T}}(\mathrm{V})$ bins and for both the 7 TeV and the 8 TeV data, are combined to obtain 95% confidence level upper limits on the product of the VH production cross section times the $\mathrm{H} \to \mathrm{b\bar{b}}$ branching ratio, with respect to the expectations for a standard model Higgs boson ($\sigma/\sigma_{\mathrm{SM}}$). The observed limits at each mass point, the median expected limits, and the 1σ and 2σ bands are calculated using the modified frequentist method CL_s [50–52]. Table 9 lists these limits, and Fig. 3 displays the results. In the mass range studied, the observed 95% CL upper limits vary from 1.1 to 3.1 times the standard model prediction, and the corresponding expected limits vary from 0.7 to 1.5. At a Higgs boson mass of 125 GeV the observed limit is 1.89 and the expected limit is 0.95. Given that the resolution for the reconstructed Higgs boson mass is $\approx 10\%$, the results are compatible with a Higgs mass of 125 GeV. This is demonstrated by the red dashed line in the figure, which is the the observed limits obtained from replacing the data with the sum of expected background and signal for a Higgs boson at a mass of 125 GeV.

For all channels an excess of events over the expected background contributions is indicated by the fits of the BDT output distributions. The probabilities (p-values) that the observed excess is due to background fluctuations alone, as a function of the Higgs boson mass hypothesis, are shown in Fig. 3. For a mass of 125 GeV the excess of observed events is 2.1 standard deviations, and is consistent with the standard model prediction for Higgs boson production. The fit also returns the most likely value of the production cross section for a 125 GeV Higgs boson, relative to the standard model cross section (signal strength), for each channel and for all channels combined. These are shown in Fig. 4. The observed signal strengths for the individual modes are consistent with each other and the value for the signal strength for all modes combined is $1.0^{+0.5}_{-0.5}$. The dependency of the combined signal strength on the value assumed for the Higgs boson masses is also shown in Fig. 4.

Fig. 5 shows a weighted dijet invariant mass distribution of for the combination of all six channels, in all $p_{\mathrm{T}}(\mathrm{V})$ bins, in the combined 7 TeV and 8 TeV data, using the event selection for the $m(\mathrm{jj})$ analysis described in section 5. For each channel, the relative weight of each $p_{\mathrm{T}}(\mathrm{V})$ bin is obtained from the ratio of the expected number of signal events to the sum of expected signal and background events in a window of $m(\mathrm{jj})$ values between 105 and 150 GeV. The expected signal used corresponds to the production of a Higgs boson with a mass of 125 GeV. The weight for the highest $p_{\mathrm{T}}(\mathrm{V})$ bin is set to 1.0 and all other weight are adjusted proportionally. Fig. 5 also shows the same weighted dijet invariant mass distribution when all backgrounds, except dibosons, are subtracted. The data are consistent with the presence of a diboson signal (ZZ and WZ, with $\mathrm{Z} \to \mathrm{b\bar{b}}$), with a rate consistent with the standard model prediction from the MADGRAPH generator, together with a small excess consistent with originating from the production of a 125 GeV standard model Higgs boson. For the $m(\mathrm{jj})$ analysis, a fit to the dijet invariant mass distribution results in a measured Higgs boson signal strength, relative to that predicted by the standard model, of $0.76^{+0.68}_{-0.66}$, with a significance of 1.1 standard deviations. For a Higgs boson of mass 125 GeV, the expected and observed 95% CL upper limits on the production cross section, relative to the standard model prediction, are 1.4 and 2.0, respectively.

As a validation of the multi-variate technique, BDT discriminants are trained using the diboson sample as signal, and all other processes, including VH production (at the predicted standard model rate for a 125 GeV Higgs mass), as background. This is done for the 8 TeV analysis only. The observed excess of events for the combined WZ and ZZ with $\mathrm{Z} \to \mathrm{b\bar{b}}$ processes is

7.5 standard deviations from what would be expected from background fluctuations alone. The corresponding signal strength, relative to the prediction from the diboson MADGRAPH generator described in Section 2, is measured to be $1.19^{+0.28}_{-023}$.

9 Conclusions

A search for the standard model Higgs boson decaying to $b\bar{b}$ when produced in association with a weak vector boson is reported for the $W(\mu\nu)H$, $W(e\nu)H$, $W(\tau\nu)H$, $Z(\mu\mu)H$, $Z(ee)H$ and $Z(\nu\nu)H$ channels. The search is performed in data samples corresponding to integrated luminosities of 5.0 fb^{-1} at $\sqrt{s} = 7$ TeV and up to 19.0 fb^{-1} at $\sqrt{s} = 8$ TeV, recorded by the CMS experiment at the LHC. Upper limits, at the 95% confidence level, on the VH production cross section times the $H \to b\bar{b}$ branching ratio, with respect to the expectations for a standard model Higgs boson, are derived for a Higgs boson in the mass range 110–135 GeV. In this range, the observed upper limits vary from 1.1 to 3.1 times the standard model prediction; the corresponding expected limits vary from 0.7 to 1.5. At a Higgs boson mass of 125 GeV the observed limit is 1.89 and the expected limit is 0.95. An excess of events is observed above the expected background with a local significance of 2.1 standard deviations, which is consistent with the expectation from the production of the standard model Higgs boson. The signal strength corresponding to this excess, relative to that of the standard model Higgs boson, is $1.0^{+0.5}_{-0.5}$.

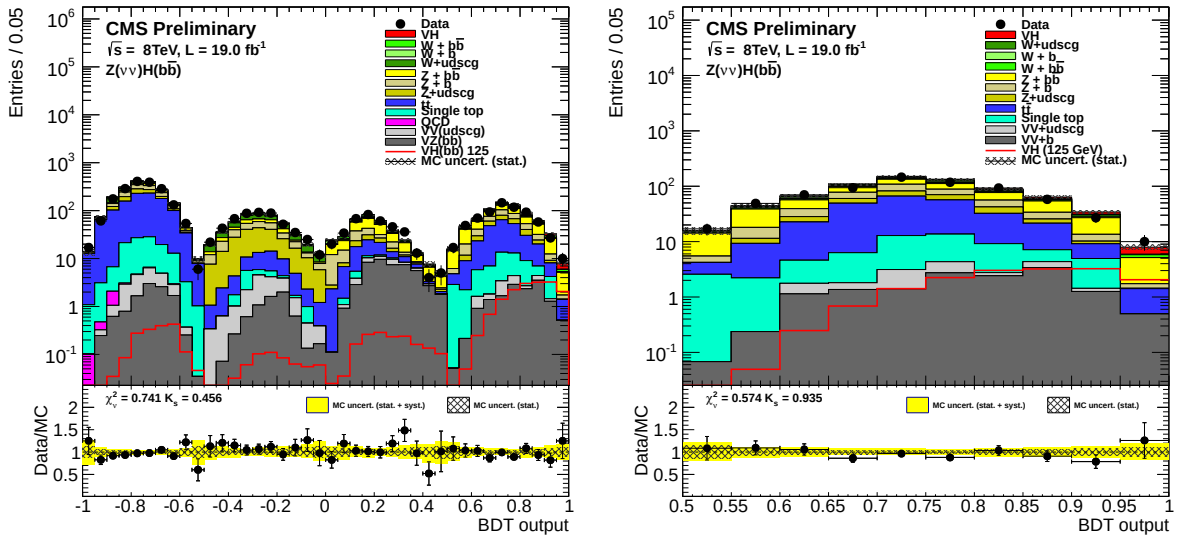

Figure 1: 8 TeV analysis. Post-fit BDT output distributions for $Z(\nu\nu)H$ in the high $p_T(V)$ bin, for data (points with errors), all backgrounds, and signal, after all selection criteria have been applied. The last partition of the high $p_T(V)$ bin is shown in more detail on the figure on the right.

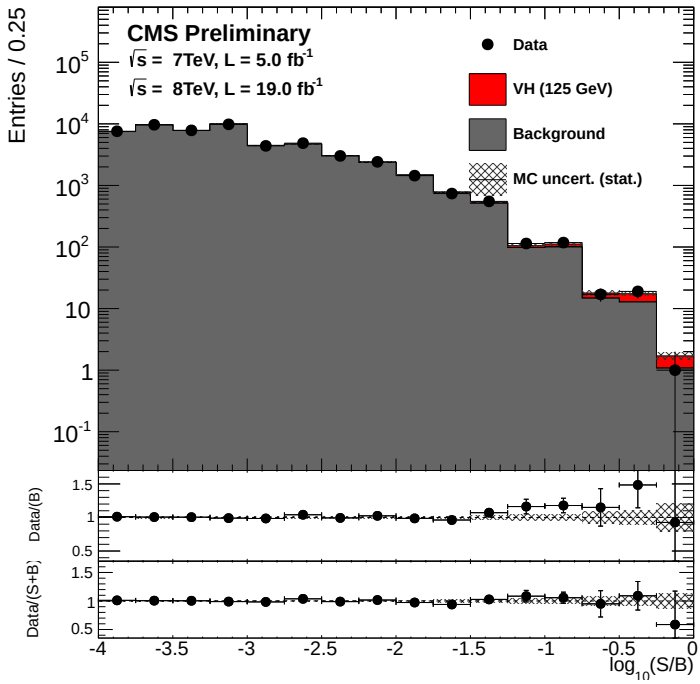

Figure 2: Combination of all BDT discriminants into a single distribution where all events, for all channels, are sorted in bins of similar expected signal-to-background ratio, as given by the value of the output of their corresponding BDT discriminant (trained with a Higgs boson mass of 125 GeV). The two bottom insets show the ratio of the data to the background-only prediction (above) and to the predicted sum of background plus signal (below).

Table 9: Expected and observed 95% CL upper limits on the product of the VH production cross section times the $H \to b\bar{b}$ branching ratio, with respect to the expectations for a standard model Higgs boson.

m_H(GeV)	110	115	120	125	130	135
BDT Exp.	0.73	0.79	0.91	0.95	1.25	1.53
BDT Obs.	1.13	1.09	1.74	1.89	2.30	3.07

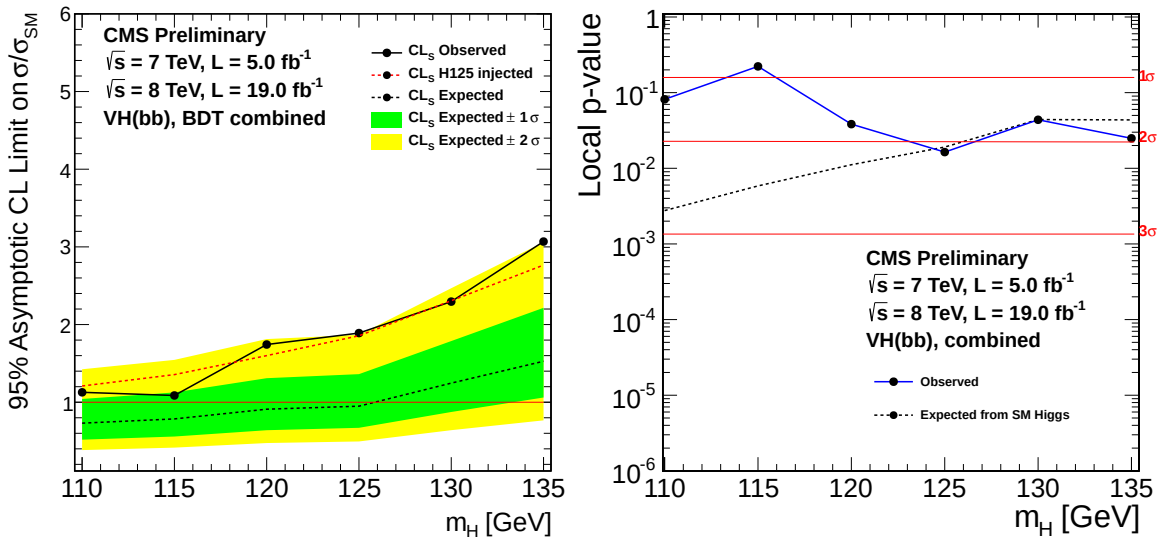

Figure 3: **Left:** Expected and observed 95% CL upper limits on the product of the VH production cross section times the $H \to b\bar{b}$ branching ratio, with respect to the expectations for a standard model Higgs boson. The limits are combined for the 2011 7 TeV and the 2012 8 TeV data. The red dashed line represents the expected observed limits obtained from replacing the data with the sum of expected background and signal for a Higgs boson at a mass of 125 GeV. **Right:** p-values for background fluctuations to account for the observed excess of events in the data

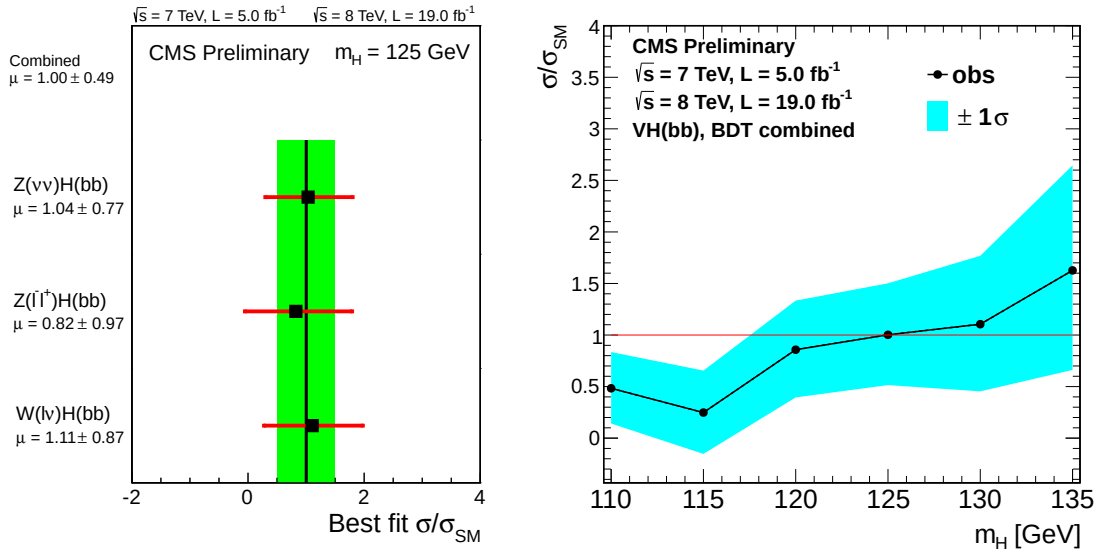

Figure 4: **Left:** the most likely value of the production cross section for a 125 GeV Higgs boson, relative to the standard model cross section, for each channel and for all channels combined (band). **Right:** combined signal strength for all modes as a function of the value assumed for the Higgs boson mass.

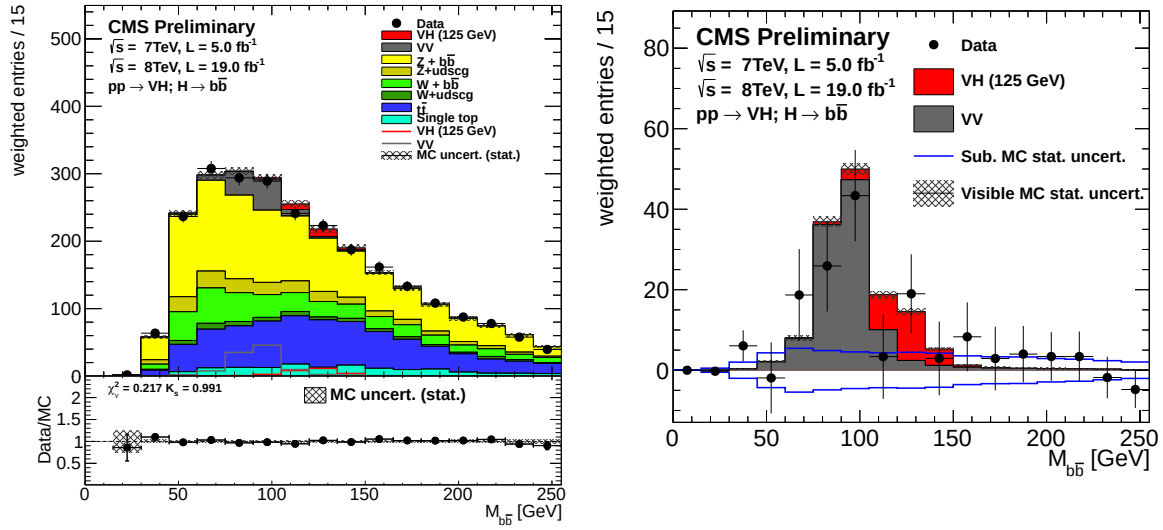

Figure 5: **Left:** weighted dijet invariant mass distribution, combined for all channels. For each channel, the relative weight of each $p_{\mathrm{T}}(\mathrm{V})$ bin is obtained from the ratio of the expected number of signal events to the sum of expected signal and background events in a window of $m(\mathrm{jj})$ values between 105 and 150 GeV. The expected signal used corresponds to the production of a Higgs boson with a mass of 125 GeV. The weight for the highest $p_{\mathrm{T}}(\mathrm{V})$ bin is set to 1.0 and all other weights are adjusted proportionally. **Right**: same distribution with all backgrounds, except dibosons, subtracted. The solid histograms for the backgrounds and the signal are summed cumulatively. The line histogram for signal and for VV backgrounds are also shown superimposed. The data is represented by points with error bars.

10 Appendix

Shown in Figs. 6–10 are all the BDT distributions, for the m_{H}= 125 GeV training, for all channels and for all $p_{\mathrm{T}}(\mathrm{V})$ bins. See section 8 for more details.

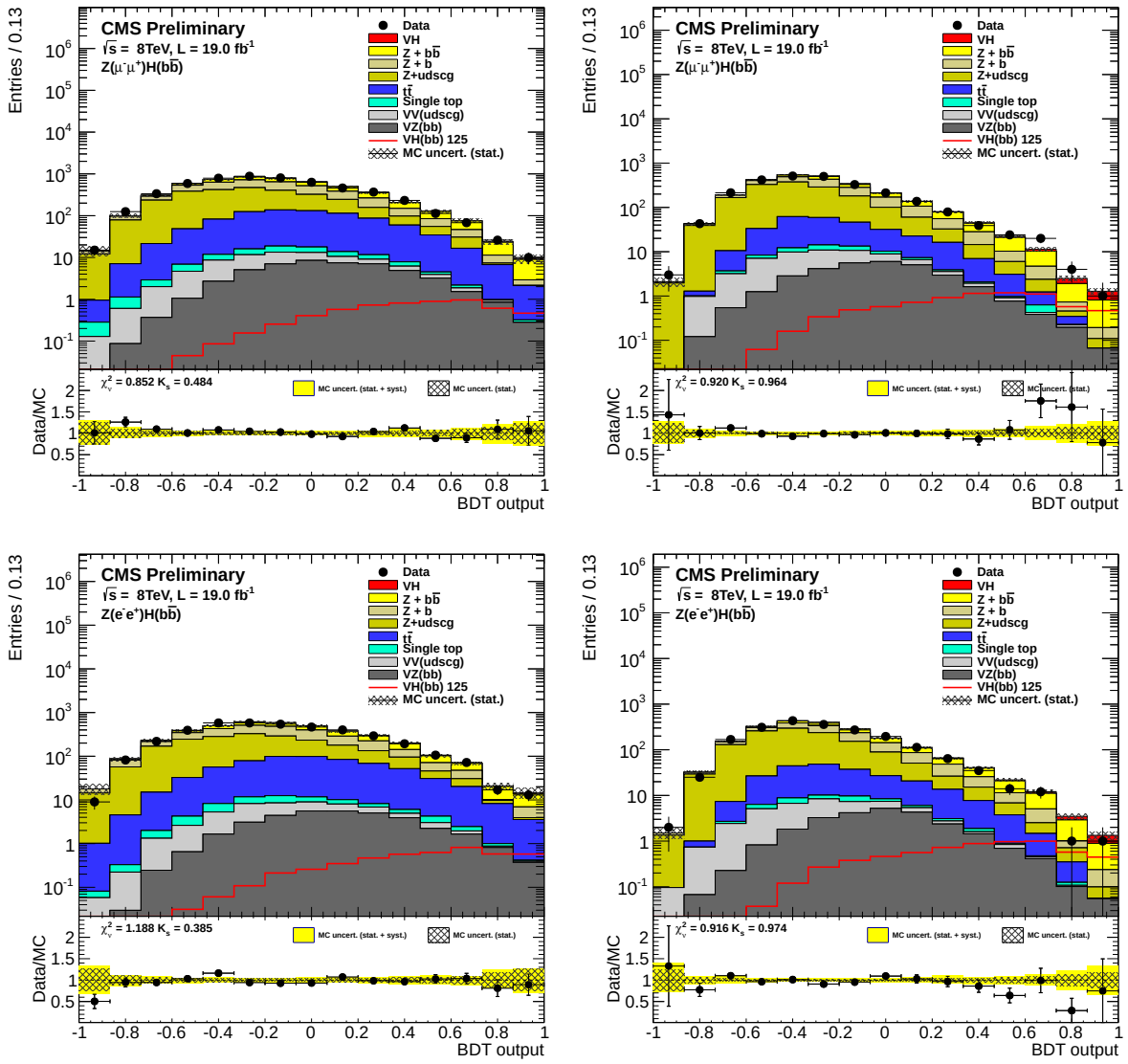

Figure 6: 8 TeV analysis. Post-fit BDT output distributions for Z($\ell\ell$)H in the low $p_{\mathrm{T}}(\mathrm{V})$ bin (left) and high $p_{\mathrm{T}}(\mathrm{V})$ bin (right), for data (points with errors), all backgrounds, and signal, after all selection criteria have been applied. Top: Z($\mu\mu$)H bottom: Z(ee)H

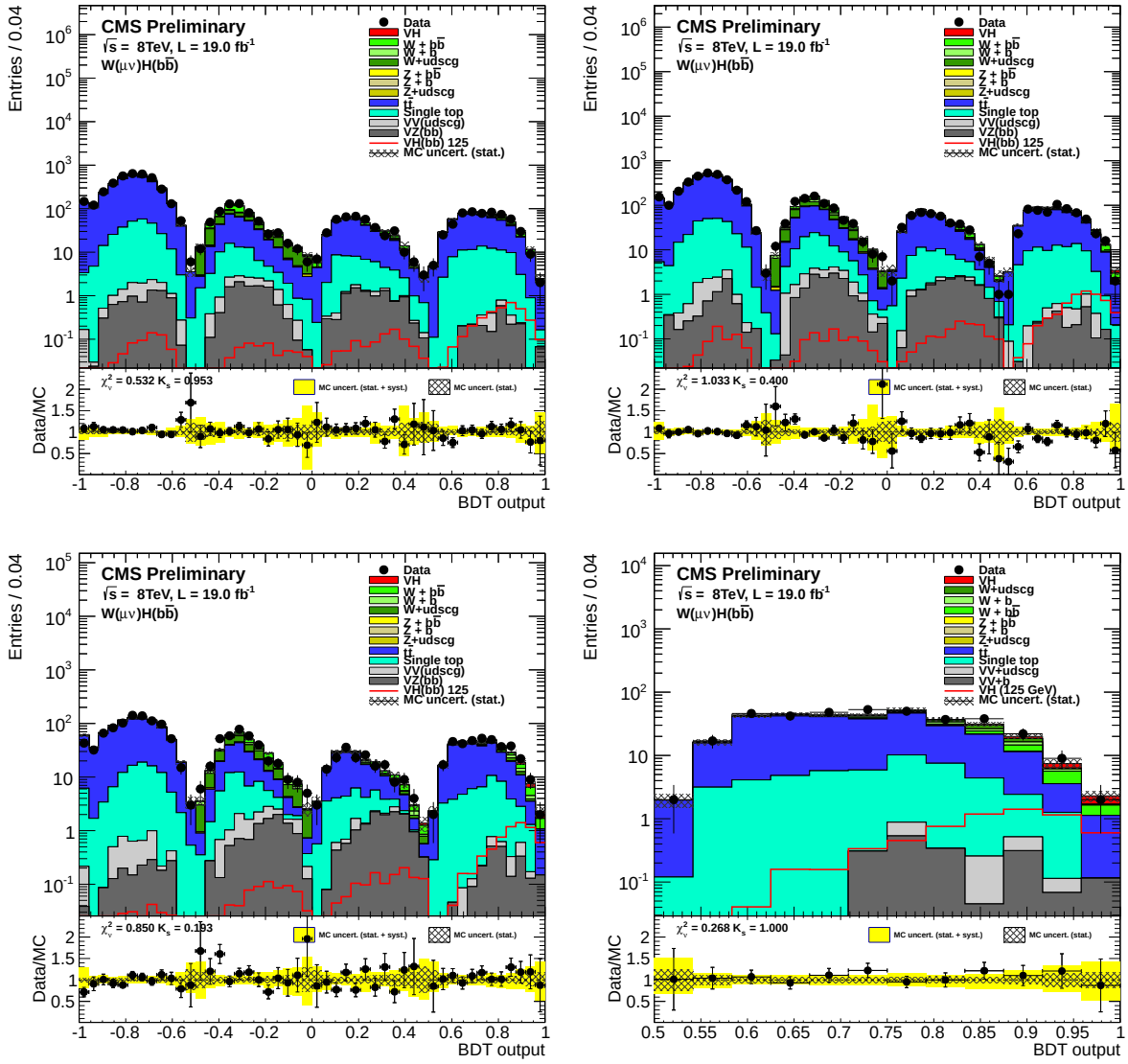

Figure 7: 8 TeV analysis. Post-fit BDT output distributions for W($\mu\nu$)H in the low $p_{\mathrm{T}}(\mathrm{V})$ bin (left), the intermediate $p_{\mathrm{T}}(\mathrm{V})$ (right), and the high $p_{\mathrm{T}}(\mathrm{V})$ (bottom), for data (points with errors), all backgrounds, and signal, after all selection criteria have been applied. Bottom right: last partition of the high $p_{\mathrm{T}}(\mathrm{V})$ bin is shown in more detail.

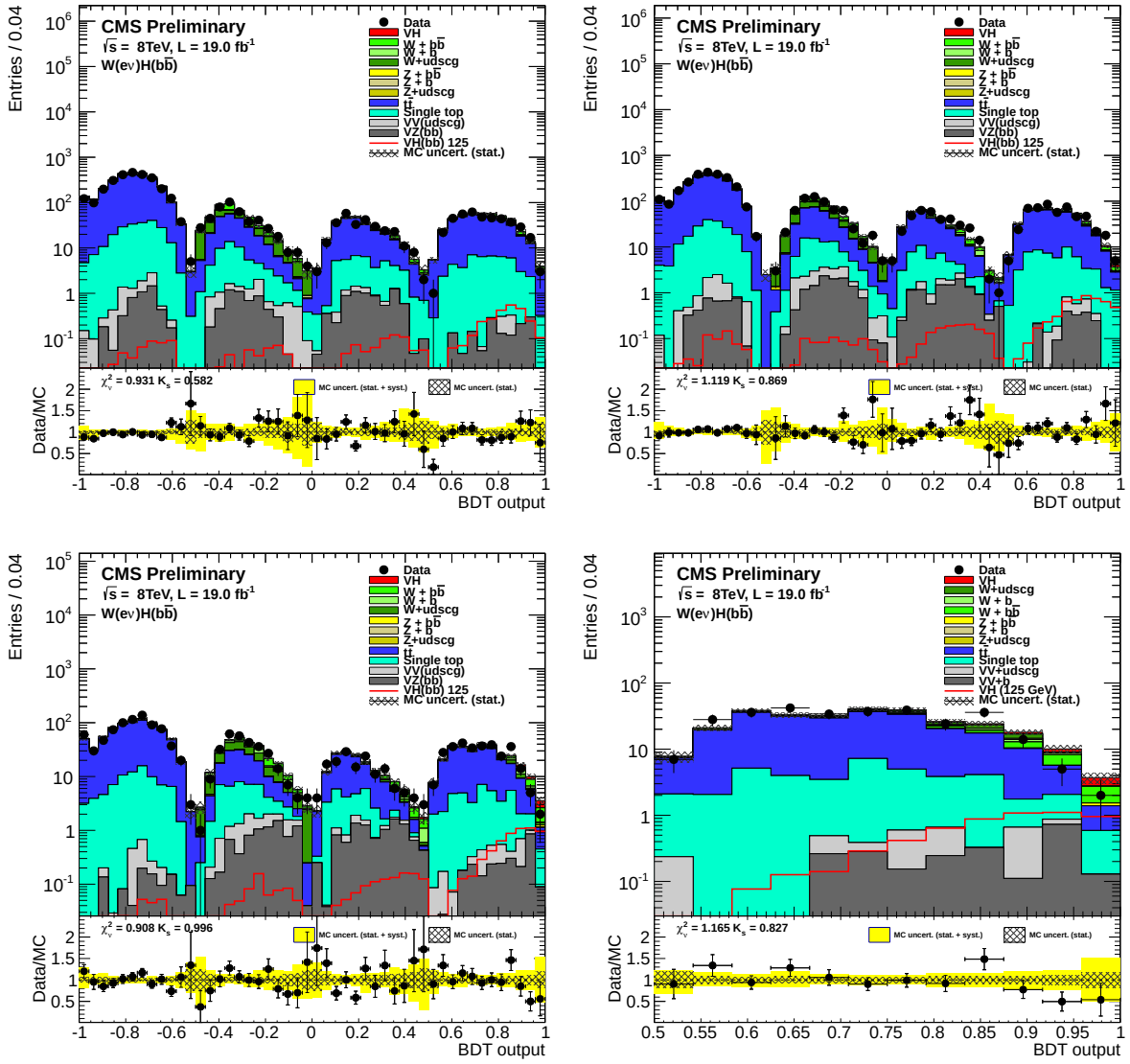

Figure 8: 8 TeV analysis. Pre-fit BDT output distributions for W($e\nu$)H in the low $p_T(V)$ bin (left), the intermediate $p_T(V)$ (right), and the high $p_T(V)$ (bottom), for data (points with errors), all backgrounds, and signal, after all selection criteria have been applied. Bottom right: the last partition of the high $p_T(V)$ bin is shown in more detail.

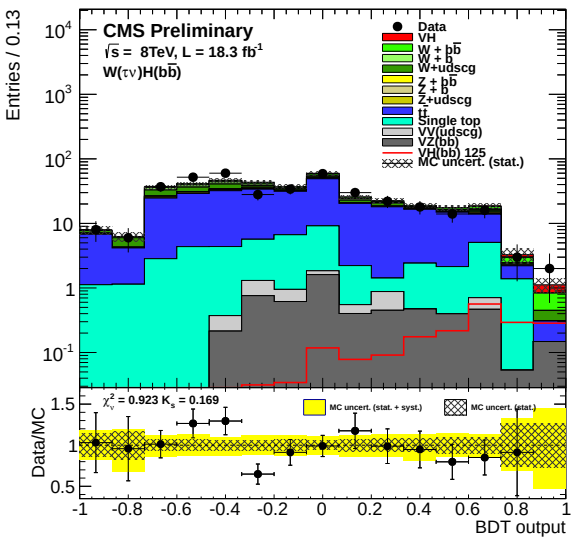

Figure 9: 8 TeV analysis. Post-fit BDT output distributions for W($\tau\nu$)H for data (points with errors), all backgrounds, and signal, after all selection criteria have been applied.

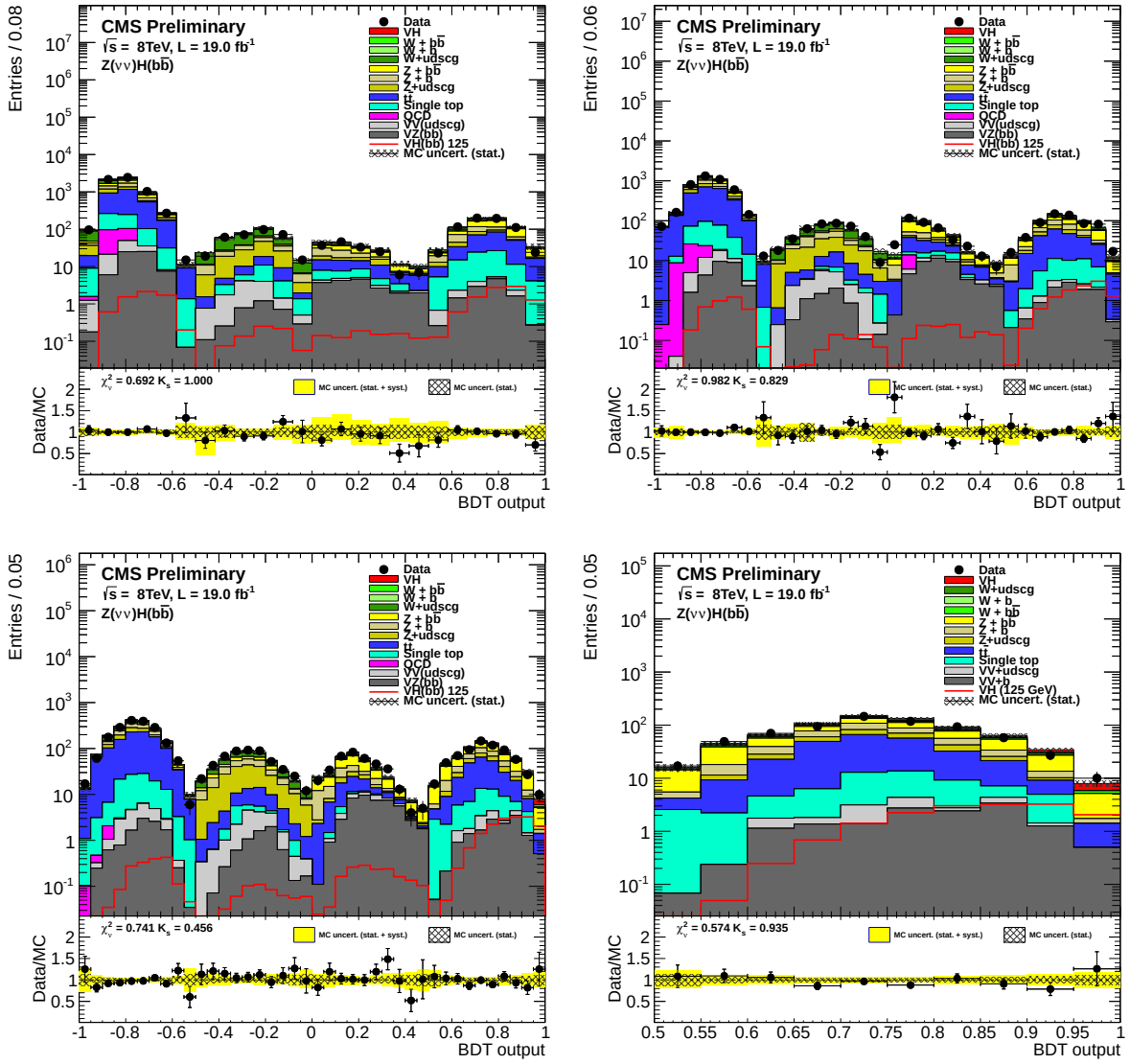

Figure 10: 8 TeV analysis. Post-fit BDT output distributions for Z($\nu\nu$)H in the low $p_{\mathrm{T}}(\mathrm{V})$ bin (left), the medium $p_{\mathrm{T}}(\mathrm{V})$ (right), and the high $p_{\mathrm{T}}(\mathrm{V})$ (bottom), for data (points with errors), all backgrounds, and signal, after all selection criteria have been applied. Bottom right: the last partition of the high $p_{\mathrm{T}}(\mathrm{V})$ bin is shown in more detail.

References

[1] ATLAS Collaboration, "Observation of a new particle in the search for the Standard Model Higgs boson with the ATLAS detector at the LHC", *Phys.Lett.B* (2012) doi:10.1016/j.physletb.2012.08.020, arXiv:1207.7214.

[2] CMS Collaboration, "Observation of a new boson at a mass of 125 GeV with the CMS experiment at the LHC", *Phys.Lett.B* (2012) doi:10.1016/j.physletb.2012.08.021, arXiv:1207.7235.

[3] F. Englert and R. Brout, "Broken symmetry and the mass of gauge vector mesons", *Phys. Rev. Lett.* **13** (1964) 321, doi:10.1103/PhysRevLett.13.321.

[4] P. W. Higgs, "Broken symmetries, massless particles and gauge fields", *Phys. Lett.* **12** (1964) 132, doi:10.1016/0031-9163(64)91136-9.

[5] P. W. Higgs, "Broken symmetries and the masses of gauge bosons", *Phys. Rev. Lett.* **13** (1964) 508, doi:10.1103/PhysRevLett.13.508.

[6] G. S. Guralnik, C. R. Hagen, and T. W. B. Kibble, "Global conservation laws and massless particles", *Phys. Rev. Lett.* **13** (1964) 585, doi:10.1103/PhysRevLett.13.585.

[7] P. W. Higgs, "Spontaneous symmetry breakdown without massless bosons", *Phys. Rev.* **145** (1966) 1156, doi:10.1103/PhysRev.145.1156.

[8] T. W. B. Kibble, "Symmetry breaking in non-Abelian gauge theories", *Phys. Rev.* **155** (1967) 1554, doi:10.1103/PhysRev.155.1554.

[9] CDF Collaboration, D0 Collaboration Collaboration, "Higgs Boson Studies at the Tevatron", arXiv:1303.6346.

[10] B. P. Roe, H.-J. Yang, and J. Zhu, "Boosted decision trees, a powerful event classifier",. Prepared for PHYSTATO5: Statistical Problems in Particle Physics, Astrophysics and Cosmology, Oxford, England, United Kingdom, 12-15 Sep 2005.

[11] CMS Collaboration, "Search for the standard model Higgs boson produced in association with W or Z bosons, and decaying to bottom quarks for HCP 2012", *CMS Physics Analysis Summary* **CMS-PAS-HIG-12-044** (2012).

[12] CMS Collaboration, "The CMS experiment at the CERN LHC", *JINST* **03** (2008) S08004, doi:10.1088/1748-0221/3/08/S08004.

[13] GEANT4 Collaboration, "GEANT4: A Simulation toolkit", *Nucl. Instrum. Meth.* **A506** (2003) 250–303, doi:10.1016/S0168-9002(03)01368-8.

[14] S. Frixione, P. Nason, and C. Oleari, "Matching NLO QCD computations with Parton Shower simulations: the POWHEG method", *JHEP* **11** (2007) 070, doi:10.1088/1126-6708/2007/11/070, arXiv:0709.2092.

[15] S. Gieseke et al., "Herwig++ 2.0 Release Note", (2006). arXiv:hep-ph/0609306.

[16] J. Alwall et al., "MadGraph 5 : Going Beyond", *JHEP* **1106** (2011) 128, doi:10.1007/JHEP06(2011)128, arXiv:1106.0522.

[17] A. Martin et al., "Parton distributions for the LHC", *Eur.Phys.J.* **C63** (2009) 189, doi:10.1140/epjc/s10052-009-1072-5, arXiv:0901.0002.

[18] J. Pumplin et al., "New generation of parton distributions with uncertainties from global QCD analysis", *JHEP* **0207** (2002) 012, arXiv:hep-ph/0201195.

[19] CMS Collaboration, "Measurement of the Underlying Event Activity at the LHC with $\sqrt{s} = 7$ TeV and Comparison with $\sqrt{s} = 0.9$ TeV", *JHEP* **1109** (2011) 109, doi:10.1007/JHEP09(2011)109, arXiv:1107.0330.

[20] CMS Collaboration, "Particle–Flow Event Reconstruction in CMS and Performance for Jets, Taus, and $E_{\mathrm{T}}^{\mathrm{miss}}$", CMS Physics Analysis Summary CMS-PAS-PFT-09-001, (2009).

[21] C. Collaboration, "Commissioning of the Particle-flow Event Reconstruction in Minimum-Bias and Jet Events from pp Collisions at 7 TeV", CMS Physics Analysis Summary CMS-PAS-PFT-10-002, (2010).

[22] M. Cacciari and G. P. Salam, "Pileup subtraction using jet areas", *Phys. Lett. B* **659** (2008) 119, doi:10.1016/j.physletb.2007.09.077, arXiv:0707.1378.

[23] M. Cacciari, G. P. Salam and G. Soyez, "The anti-k_t jet clustering algorithm", *JHEP* **04** (2008) 063, doi:10.1088/1126-6708/2008/04/063, arXiv:0802.1189.

[24] M. Cacciari, G. P. Salam, and G. Soyez, "FastJet User Manual", *Eur.Phys.J.* **C72** (2012) 1896, doi:10.1140/epjc/s10052-012-1896-2, arXiv:1111.6097.

[25] M. Cacciari and G. P. Salam, "Dispelling the N^3 myth for the k_t jet-finder", *Phys. Lett. B* **641** (2006) 57–61, doi:10.1016/j.physletb.2006.08.037, arXiv:hep-ph/0512210.

[26] CMS Collaboration, "Determination of Jet Energy Calibration and Transverse Momentum Resolution in CMS", *JINST* **06** (2011) 11002, doi:10.1088/1748-0221/6/11/P11002.

[27] CMS Collaboration, "Electron reconstruction and identification at $\sqrt{s} = 7$ TeV", *CMS Physics Analysis Summary* **CMS-PAS-EGM-10-004** (2010).

[28] CMS Collaboration, "Performance of CMS muon reconstruction in pp collision events at sqrt(s) = 7 TeV", *JINST* **7** (2012) P10002, doi:10.1088/1748-0221/7/10/P10002, arXiv:1206.4071.

[29] CMS Collaboration, "Performance of τ-lepton reconstruction and identification in CMS", *JINST* **7** (2012) P01001, doi:10.1088/1748-0221/7/01/P01001.

[30] CMS Collaboration Collaboration, "Identification of b-quark jets with the CMS experiment", *JINST* **8** (2013) P04013, doi:10.1088/1748-0221/8/04/P04013, arXiv:1211.4462.

[31] J. M. Butterworth et al., "Jet Substructure as a New Higgs-Search Channel at the Large Hadron Collider", *Phys. Rev. Lett.* **100** (2008) 242001, doi:10.1103/PhysRevLett.100.242001.

[32] T. Aaltonen et al., "Improved b-jet Energy Correction for $H \to b\bar{b}$ Searches at CDF", (2011). arXiv:1107.3026.

[33] CDF Collaboration, "Search for the Standard Model Higgs Boson Decaying to a $b\bar{b}$ Pair in Events with Two Oppositely Charged Leptons Using the Full CDF Data Set", *Phys. Rev. Lett.* **109** (Sep, 2012) 111803, doi:10.1103/PhysRevLett.109.111803.

[34] J. Gallicchio and M. D. Schwartz, "Seeing in Color: Jet Superstructure", *Phys. Rev. Lett.* **105** (Jul, 2010) 022001, doi:10.1103/PhysRevLett.105.022001.

[35] CMS Collaboration, "Measurement of B hadron angular correlations in association to a Z boson", *CMS Physics Analysis Summary* **CMS-PAS-EWK-11-015** (2012). Submitted for publication.

[36] ATLAS Collaboration, "Measurement of the cross-section for W boson production in association with b-jets in pp collisions at sqrt(s) = 7 TeV with the ATLAS detector", arXiv:1302.2929.

[37] CMS Collaboration, "Absolute Calibration of the CMS Luminosity Measurement: Summer 2011 Update", *CMS Physics Analysis Summary* **CMS-PAS-EWK-11-001** (2011).

[38] CMS Collaboration, "Absolute Calibration of the Luminosity Measurement at CMS: Winter 2012 Update", *CMS Physics Analysis Summary* **CMS-PAS-SMP-12-008** (2012).

[39] LHC Higgs Cross Section Working Group et al., "Handbook of LHC Higgs Cross Sections: 1. Inclusive Observables", *CERN-2011-002* (CERN, Geneva, 2011) arXiv:1101.0593.

[40] M. Botje et al., "The PDF4LHC Working Group Interim Recommendations", arXiv:1101.0538.

[41] S. Alekhin et al., "The PDF4LHC Working Group Interim Report", arXiv:1101.0536.

[42] H. Lai et al., "New parton distributions for collider physics", *Phys. Rev.* **D82** (2010) 074024, doi:10.1103/PhysRevD.82.074024, arXiv:1007.2241.

[43] R. D. Ball et al., "Impact of Heavy Quark Masses on Parton Distributions and LHC Phenomenology", *Nucl.Phys.* **B849** (2011) 296–363, doi:10.1016/j.nuclphysb.2011.03.021, arXiv:1101.1300.

[44] M. Ciccolini et al., "Strong and electroweak corrections to the production of Higgs+2jets via weak interactions at the LHC", *Phys. Rev. Lett.* **99** (2007) 161803, doi:10.1103/PhysRevLett.99.161803, arXiv:0707.0381.

[45] M. Ciccolini, A. Denner, and S. Dittmaier, "Electroweak and QCD corrections to Higgs production via vector-boson fusion at the LHC", *Phys. Rev.* **D77** (2008) 013002, doi:10.1103/PhysRevD.77.013002, arXiv:0710.4749.

[46] A. Denner et al., "Electroweak corrections to Higgs-strahlung off W/Z bosons at the Tevatron and the LHC with HAWK", *JHEP* **1203** (2012) 075, doi:10.1007/JHEP03(2012)075, arXiv:1112.5142.

[47] G. Ferrera, M. Grazzini, and F. Tramontano, "Associated WH production at hadron colliders: a fully exclusive QCD calculation at NNLO", arXiv:1107.1164.

[48] CMS Collaboration, "Measurement of the single-top t-channel cross section in pp collisions at centre-of-mass energy of 8 TeV", *CMS Physics Analysis Summary* **CMS-PAS-TOP-12-011** (2012).

[49] CMS Collaboration, "Measurement of W+W- and ZZ production cross sections in pp collisions at sqrt(s) = 8 TeV", *Phys.Lett.* **B721** (2013) 190–211, doi:10.1016/j.physletb.2013.03.027, arXiv:1301.4698.

[50] A. L. Read, "Presentation of search results: the CLs technique", *J. Phys. G* **28** (2002), no. 10, 2693, doi:10.1088/0954-3899/28/10/313.

[51] T. Junk, "Confidence level computation for combining searches with small statistics", *Nucl. Instrum. Meth.* **A434** (1999) 435, doi:10.1016/S0168-9002(99)00498-2.

[52] ATLAS and CMS Collaborations, LHC Higgs Combination Group, "Procedure for the LHC Higgs boson search combination in Summer 2011", ATL-PHYS-PUB/CMS NOTE 2011-11, 2011/005, (2011).